Film Trapping Technique: Precise Method for Three-Phase Contact Angle Determination of Solid and Fluid Particles of Micrometer Size

Asen Hadjiiski,[†] Roumiana Dimova,[†] Nikolai D. Denkov,*,[†] Ivan B. Ivanov,[†] and Rajendra Borwankar[‡]

Laboratory of Thermodynamics and Physico-chemical Hydrodynamics, Faculty of Chemistry, Sofia University, 1126 Sofia, Bulgaria, and Kraft General Foods, Inc., Technology Center, 801 Waukegan Road, Glenview, Illinois 60025

Received June 6, 1996. In Final Form: August 29, 1996[⊗]

A novel method for determination of the three-phase contact angle at the surface of a micrometer-sized particle (latex sphere, oil droplet, or biological cell) is described. The particle is entrapped within a liquid film of equilibrium thickness smaller than the particle diameter. Thus a liquid meniscus (a layer of uneven thickness) is formed around the particle. When observed in reflected monochromatic light, this meniscus appears as an interference pattern of concentric bright and dark fringes. From the radii of the interference fringes, one can restore the meniscus shape by using the solution of the Laplace equation of capillarity. In this way the three-phase contact angle of the particle and the capillary pressure can be determined. We demonstrate the applicability of our method to latex spheres from several batch samples (between 1 and 7 μm in diameter) and to oil droplets, stabilized by adsorbed protein layer. The numerical procedures used for contact angle determination are described, and illustrative results are presented and discussed.

Introduction

The three-phase contact angle is an important characteristic of colloidal particles, because it represents a quantitative measure of the hydrophobicity of their surfaces. The hydrophilic particles possess contact angle particle−water−air (or particle−water−oil) close to zero, while the hydrophobic particles have contact angles around 90° and above.

The hydrophobic character of the particles is important when their interaction with oil−water and air−water interfaces, as well as with lipid bilayers, is considered.[1] The hydrophobic particles and surfaces demonstrate[1,2] a strong, long-range attractive force (referred to as "hydrophobic force") whose origin is still poorly understood.[2] The adsorption of protein and surfactant molecules on latex spheres is also strongly dependent on the hydrophobicity of the particles.[3]

When colloidal particles are attached to a fluid interface, a long-range capillary interaction may appear between them, due to the deformation of the interface around the particles.[4] As shown recently,[5−8] this force is particularly strong when the colloidal particles are partially immersed in a liquid layer of thickness smaller than the particle diameter and may lead to the formation of two-dimensional, well-ordered particle arrays[8] (2D colloidal crystals). The calculations[4−6] and the experiments[7] demonstrated that the magnitude of the capillary force is strongly dependent on the particle contact angle.

It was recognized long ago that the magnitude of the three-phase contact angle is of crucial importance for the efficiency of solid particles in several industrial applications. Two well-known examples are (i) antifoaming formulations containing hydrophobic particles[9−11] and (ii) emulsions stabilized by solid particles[12−16] (so-called "Pickering[17] emulsions"). The experiments and theory show[9−11] that antifoaming formulations containing solid particles of *larger* contact angle are more effective. On the other hand, contact angles *smaller than* (but close to) 90° were found to be most favorable for the formation of *oil−in−water* Pickering emulsions, while angles *larger than* 90° lead to *water−in−oil* emulsions.[12−15] The magnitude of the particle contact angle determines the strength of particle attachment to air bubbles in another important technological process, *froth flotation*, which is widely used for separation of minerals and ores.[18]

The significance of the particle three-phase contact angle for these and other industrial applications has stimulated the development of several methods for contact angle determination. In some procedures[19,20] the particles are pressed to form tablets or impermeable continuous layers

---

* To whom correspondence should be addressed: phone: (+359) 2-962 5310; fax, (+359) 2-962 5643; e-mail, denkov@Ltph.cit.bg.

[†] Sofia University.

[‡] Kraft General Foods, Inc.

[⊗] Abstract published in *Advance ACS Abstracts,* November 15, 1996.

(1) Ducker, W. A.; Xu, Z.; Israelachvili, J. N. *Langmuir* **1994**, *10*, 3279.

(2) Israelachvili, J. N. *Intermolecular and Surface Forces,* 2nd ed.; Academic Press: New York, 1992.

(3) Yoon, J.-Y.; Park, H.-Y.; Kim, J.-H.; Kim, W.-S. *J. Colloid Interface Sci.* **1996**, *177*, 613.

(4) Chan, D. Y. C.; Henry, J. D.; White, L. R. *J. Colloid Interface Sci.* **1981**, *79*, 410.

(5) Kralchevsky, P. A.; Paunov, V. N.; Denkov, N. D.; Ivanov, I. B.; Nagayama, K. *J. Colloid Interface Sci.* **1993**, *155*, 420.

(6) Kralchevsky, P. A.; Nagayama, K. *Langmuir* **1994**, *10*, 23.

(7) Velev, O. D.; Denkov, N. D.; Paunov, V. N.; Kralchevsky, P. A.; Nagayama, K. *Langmuir* **1993**, *9*, 3702.

(8) Denkov, N. D.; Velev, O. D.; Kralchevsky, P. A.; Ivanov, I. B.; Yoshimura, H.; Nagayama, K. *Langmuir* **1992**, *8*, 3183; *Nature* **1993**, *361*, 26.

(9) Garrett, P. R. In *Defoaming: Theory and Industrial Applications*; Garrett, P. R., Ed.; Surfactant Science Series, Vol. 45; Marcel Dekker: New York, 1993; pp 1−117.

(10) Dippenaar, A. *Int. J. Mineral Process.* **1982** *9*, 1.

(11) Aveyard, R.; Cooper, P.; Fletcher, P. D. I.; Rutherford, C. E. *Langmuir* **1993**, *9*, 604.

(12) Schulman, J. H.; Leja, J. *Trans. Faraday Soc.* **1954**, *50*, 598.

(13) Menon, V. B.; Nikolov, A. D.; Wasan, D. T. *J. Colloid Interface Sci.* **1988**, *124*, 317.

(14) Tambe, D. E.; Sharma, M. M. *Adv. Colloid Interface Sci.* **1994**, *52*, 1.

(15) Denkov, N. D.; Ivanov, I. B.; Kralchevsky, P. A.; Wasan, D. T. *J. Colloid Interface Sci.* **1992**, *150*, 589.

(16) Levine, S.; Bowen, B. D. *Colloids Surfaces A: Physicochem. Eng. Aspects* **1993**, *70*, 33.

(17) Pickering, S. U. *J. Chem. Soc.* **1907**, *91*, 2001.

(18) Leja, J. *Surface Chemistry of Froth Flotation*; Plenum Press: New York, 1982.

(19) Jouany, C.; Chassin, P. *Colloids Surf.* **1987**, *27*, 289.

(20) van Oss, C. J.; Giese, R. F.; Costanzo, P. M. *Clays Clay Miner.* **1990**, *38*, 151.

S0743-7463(96)00555-0 CCC: $12.00

on substrates. Then the classical goniometric method is applied to determine the contact angle of liquid with tablet or layer surfaces. There are two main problems with these procedures: (i) the particles are mechanically treated to form a suitable macroscopic surface (tablet or layer), which can modify the particle surface and create a systematic error in the measurement; (ii) many particles do not form a macroscopic surface appropriate for measurement. Another method[21−23] relies on measuring the velocity of liquid penetration through a dry porous plug of particles. This method is not easily applied and encounters a number of difficulties discussed in the literature.[23]

During the last years two other methods for particle contact angle determination were developed.[24−31] In one of them[24−27] the contact angle is directly measured by taking a photograph of particle, attached to the air−water interface. This method is applicable to particles of diameter larger than ca. 20 μm and for not-too-small contact angles. Otherwise, the optical microscopy is not able to resolve precisely the position of the three-phase contact line, which is necessary for calculating the contact angle. The other method[28−31] is based on the measurement of the two-dimensional *collapse* pressure of a particle monolayer, which is spread on a liquid substrate in a Langmuir trough. The main advantage of this method is that, in principle, it is applicable to particles of nanometer size. Problems arise from the necessity to form a spread particle monolayer (which is not always possible),[30] as well as from the fact that the data interpretation often requires accounting for other effects, such as interparticle interactions[25,29,30] and line-tension.[31] In several experiments with large particles[25] (when direct measurement of the contact angle was possible) substantial deviation of the contact angle, determined by the collapse pressure method, from the directly measured contact angle, was found.

The brief literature overview presented above shows that a precise method for determination of the three-phase contact angle of particles in the micrometer range is still absent. This fact has stimulated us to develop a direct method for measuring the contact angle of micrometer particles. We demonstrate that the method (called by us the film trapping technique, FTT, see Figure 1) is applicable to spherical solid particles of diameters between ca. 1 and 10 μm. The accuracy of the method is found to be within ±2−5°. Furthermore, FTT is extended to measuring the contact angles of deformable (fluid) particles, such as oil droplets and biological cells (see Figure 2). In this case the contact angle between the microscopic liquid film (formed in the region of contact of the particle with the air−water or oil−water interface) and the surrounding meniscus is measured. According to the thermodynamics of thin liquid films,[32−35] the contact angle film-meniscus can be used to determine the adhesive

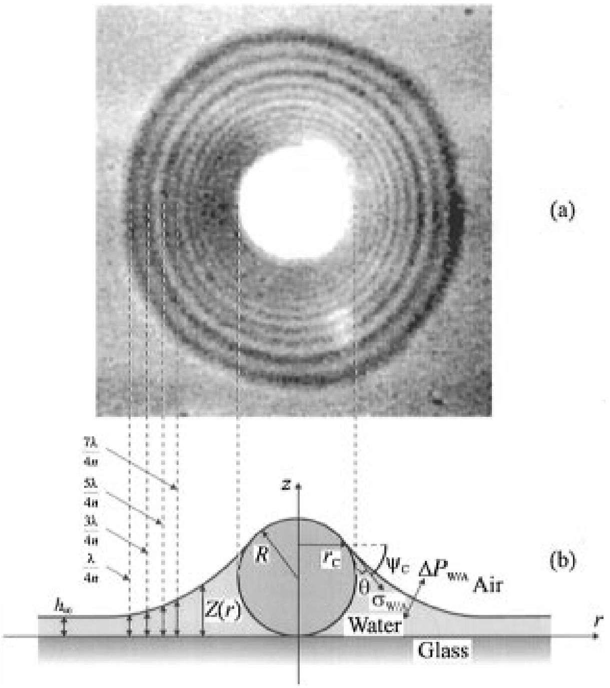

Figure 1. Basic scheme of the film trapping technique (the case of a solid sphere entrapped in a wetting film on solid substrate is illustrated). (a) When observed in reflected monochromatic light, a set of alternating dark and bright fringes appears around the particle. (b) This pattern is created by the interference of the two light beams reflected from the water−air and the water−glass interfaces. As explained in the text, from the radius of the interference fringes one can restore the shape of the liquid meniscus around the particle and to calculate the three-phase contact angle, θ.

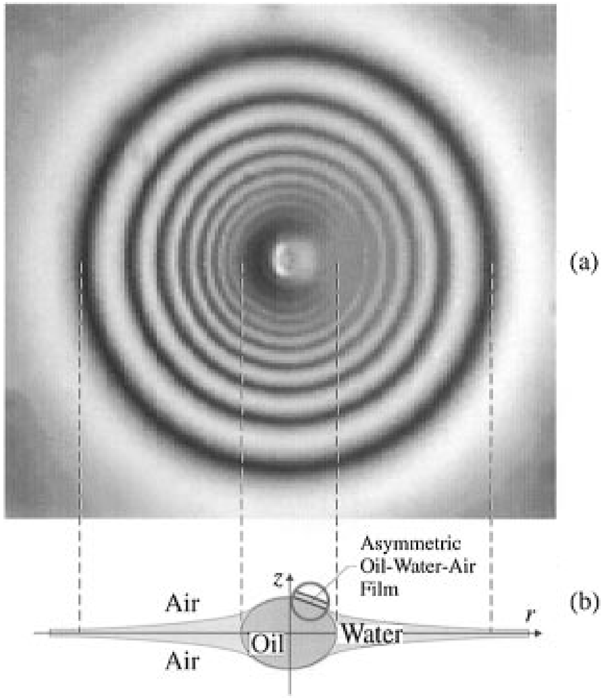

Figure 2. Oil droplet entrapped in symmetrical foam film. (a) Photograph of the droplet in reflected monochromatic light. (b) Schematic cross section of the deformed drop and the surrounding meniscus.

---

[21] Crawford, R.; Koopal, L. K.; Ralston, J. *Colloids Surf.* **1987**, *27*, 57.

[22] Chibowski, E.; Holisz, L. *Langmuir* **1992**, *8*, 710.

[23] Li, Z.; Giese, R. F.; van Oss, C. J.; Yvon, J.; Cases, J. *J. Colloid Interface Sci.* **1993**, *156*, 279.

[24] Tschaljovska, S. D.; Aleksandrova, L. B. *Chem. Technol.* **1978**, *30*, 301.

[25] Hórvölgyi, Z.; Németh, S.; Fendler, J. H. *Colloids Surf.* **1993**, *71*, 327. Hórvölgyi, Z.; Németh, S.; Fendler, J. H. *Langmuir* **1996**, *12*, 997.

[26] Velev, O. D.; Denkov, N. D.; Paunov, V. N.; Kralchevsky, P. A.; Nagayama, K. *J. Colloid Interface Sci.* **1994**, *167*, 66.

[27] Petkov, J. T.; Denkov, N. D.; Danov, K. D.; Velev, O. D.; Aust, R.; Durst, F. *J. Colloid Interface Sci.* **1995**, *172*, 147.

[28] Clint, J. H.; Taylor, S. E. *Colloids Surf.* **1992**, *65*, 61.

[29] Clint, J. H.; Quirke, N. *Colloids Surfaces A: Physicochem. Eng. Aspects* **1993**, *78*, 277.

[30] Aveyard, R.; Binks, B. P.; Fletcher, P. D. I.; Rutherford, C. E. *Colloids Surf. A: Physicochem. Engin. Aspects* **1994**, *83*, 89.

[31] Aveyard, R.; Clint, J. H. *J. Chem. Soc., Faraday Trans.* **1996**, *92*, 85.

[32] Ivanov, I. B.; Toshev, B. V. *Colloid Polym. Sci.* **1974**, *252*, 558 and 593.

Table 1. Physicochemical Properties of the Studied Latex Spheres[a]

batch no.	latex type	particle diameter (μm)	surface density of ionizable groups (μC/cm^2)	ζ-potential (mV)	contact angle (deg)
440	sulfate	1.6 (±2.5%)	9.3	-120 ± 2	56 ± 5
10-367-23	sulfate	2.1 (±6.9%)	7.9	-119 ± 2	61 ± 4
2-351-82	chloromethyl/sulfate	1.55 (±4.5%)	4.5	-94 ± 2	32 ± 4
592,1	aldehyde/sulfate	1.1 (±2.7%	12	-82 ± 2	54 ± 3
472	carboxylate-modified latex (CML)	3.1 (±5.8%)	230.4	-71 ± 2 (pH = 6) -65 ± 5 (pH = 10.8)	58 ± 2 (pH = 6) 55 ± 3 (pH = 10.8)
Dyno-spheres POL-372	sulfate	7.1	*b*	-110 ± 2	41 ± 5

[a] The batch number, latex type, particle diameter, and surface density of ionizable groups are quoted as certified by the producer. The ζ-potential and the contact angle are measured as described in the text. [b] Not available.

energy of the fluid particle to the interface. As far as we know this is the first experimental technique which allows the determination of the thermodynamic characteristics (such as contact angle film-meniscus, film tension, disjoining pressure, etc.) of micrometer-sized liquid films. In principle, the method can be further extended to allow determination of dynamic contact angles—advancing and receding ones.

The article is organized as follows. The Experimental Section describes the used materials and experimental procedures. The next section presents the numerical algorithms for data interpretation and calculation of the three-phase contact angle. The cases of solid sphere and deformable droplet are separately considered, because the geometrical configuration and the numerical procedures are different. Illustrative results with latex particles and oil droplets are afterward presented and discussed.

Experimental Section

Materials. Five samples of latex particles produced by Interfacial Dynamic Corp. (Oregon, USA) are studied. The main physicochemical characteristics of the particles are presented in Table 1. The particle diameter varies between 1.1 and 3.1 μm. Along with the batch number, latex type, diameter, and surface density of ionizable groups, given by the producer, Table 1 includes data about the particle ζ-potential and contact angle, which were measured by us and will be discussed below. In another set of experiments the contact angle of Dynospheres (type POL-372) of diameter 7.1 μm was measured (Table 1). In most of the experiments the particles were entrapped in a wetting film made from 0.01 M NaCl solution (Merck, analytical grade) at pH = 6.0 ± 0.5. The electrolyte (NaCl) was added to the suspension in order to maintain fixed ionic strength. The stock of NaCl was heated before preparing the solutions for 5 h at 450 °C for drying and removal of organic impurities. In one set of experiments the wetting film was made from 5×10^{-4} M NaOH solution (pH = 10.8 ± 0.1).

We studied also drops of purified soybean oil (containing 0.1 wt % oleic acid as additive) dispersed in aqueous solution of lyophilized bovine serum albumin (Sigma, essentially fatty acid free). The composition of the protein solution was 2.0 wt % bovine serum albumin (BSA), 0.15 M NaCl, and 0.01 M phosphate buffer of pH 6.6.

White blood cells (WBC) of a healthy male human were used to demonstrate the feasibility of the method with biological cells. Cell suspension containing a mixture of mononuclear WBC of concentration 3×10^6 mL^{-1} in RPMI was initially prepared. The liquid film (in which the cells were entrapped for investigation) was formed from a 1:1 mixture of the cell suspension with protein solution containing 3 mg/mL BSA, 3 mg/mL human IgG, and 0.05 M glycin buffer of pH = 9.2.

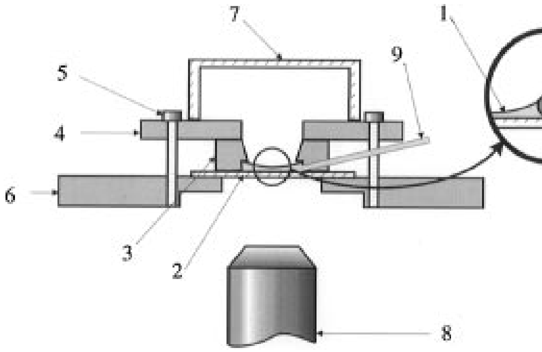

Figure 3. Experimental cell used for contact angle determination of particles entrapped in wetting films: (1) latex suspension; (2) glass plate; (3) Teflon ring; (4) metal plate; (5) screws; (6) microscope table; (7) glass cover; (8) microscope objective; (9) capillary.

All solutions were prepared with water obtained from a Milli-RO4/Milli-Q Organex water purification system (Millipore). The experiments were performed at room temperature, 24 ± 1 °C.

Experimental Cells and Procedures for Contact Angle Measurement. *Solid Spheres.* The experimental cell for measuring the contact angle of solid spheres (see Figure 3) is essentially the same as that used for controlled formation of two-dimensional latex crystals on substrates.[8] A drop of latex suspension (1 in Figure 3) is placed upon a glass plate (2). The suspension spreads over the accessible glass area, which is encircled by a Teflon ring (3). This ring is pressed against the glass by a metal plate (4) and screws (5) to avoid leakage of the liquid. The cell is mounted on the table (6) of an inverted (metallographic) type of microscope and is covered by a glass cover (7). The observations are performed from below in reflected monochromatic light (wavelength $\lambda_0 = 546$ nm). To reduce the intensity of the light reflected from the bottom glass surface (which is the main source of a background intensity) and, thereby, to increase the contrast of the image, an immersion type of objective, Plan Neofluar (8) of magnification ×40, was used.

The typical particle concentration in the used suspensions is about 1 vol %. When placed in the experimental cell, the suspension layer acquires a concave shape, so that the thinnest part of the layer is in the central part.[8] The amount of suspension in the cell, and thereby the corresponding layer thickness, is controlled by means of the capillary (9), in Figure 3, connected to a syringe. The latter is controlled by a micrometric screw. When the water layer thickness in the center of the substrate becomes smaller than the particle diameter, the particles protrude through the water–air interface and a meniscus of axial symmetry is formed around each of them. Thus the particles get trapped in a thin wetting film of uneven thickness. When observed in reflected monochromatic light, the meniscus around each particle appears as a set of concentric dark and bright fringes; see Figure 1. Each dark (bright) fringe is due to negative (positive) interference of the two light beams which are reflected from the upper, water–air, and from the lower, water–glass, interfaces, respectively. The transition from one dark to the closest bright fringe (and vice versa) corresponds to difference in the water layer thickness equal to $\lambda_0/4n_W = 102$ nm (λ_0 is the light wavelength and n_W is the refractive index of the liquid). The interference picture is observed and recorded by a CCD camera

---

(33) Kralchevsky, P. A.; Ivanov, I. B. *Chem. Phys. Lett.* **1985**, *121*, 111 and 116.

(34) de Feijter, J. In *Thin Liquid Films*; Ivanov, I. B., Ed.; Marcel Dekker: New York, 1988; Chapter 1. Ivanov, I. B.; Kralchevsky, P. A. *Ibid.*, Chapter 2.

(35) Kralchevsky, P. A.; Danov, K. D.; Ivanov, I. B. In *Foams: Theory, Measurements, and Applications*; Prud'homme, R. K., Khan, S. A., Eds.; Marcel Dekker: New York, 1995; Chapter 1.

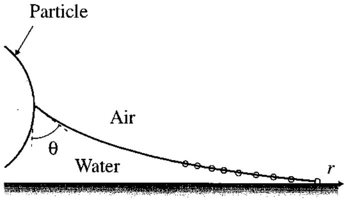

Figure 4. Reconstituted profile of the meniscus (the curve) around the solid latex sphere photographed in Figure 1a. The experimental points correspond to the positions of the maxima and minima in the intensity of the reflected light as determined from the digitized image. Only the nine outer fringes are used in the calculations, because their radii can be precisely determined from this image. $R = 3.55\ \mu$m, $\theta = 41°$.

(Panasonic WV BP500) and videorecorder. The video records are afterward used for restoration of the shape of the liquid layer around the particles and for calculation of their contact angle.

Oil Droplet (Biological Cell) in Foam Film. The oil droplets (or biological cells) are entrapped in horizontal symmetrical foam film air−liquid−air made from oil-in-water emulsion (or cell suspension); see Figure 2. The film is formed in a biconcave drop, placed in a vertical cylindrical glass capillary, by sucking out the liquid through an orifice in the capillary wall.[36] The amount of liquid in the capillary, and the capillary pressure of the meniscus, can be varied by a pressure control system. The droplets (or the biological cells) entrapped in the foam film are observed from above (microscope Axioplan Zeiss, objective LD Epiplan ×50) in reflected monochromatic light of wavelength λ_0 = 546 nm. The interference pattern appearing around each oil drop (cell) entrapped in the film is observed and recorded by a CCD camera and video recorder as described above.

The *foam* films must be stabilized by appropriate surface active substance. We found that for our purpose proteins were more suitable as film stabilizers compared to low molecular surfactants. The experiments showed that in a foam film, stabilized by low molecular surfactants, it was very difficult (and usually impossible) to entrap oil droplets, because the droplets escaped into the thicker Gibbs−Plateau border, surrounding the film, during the film formation process. When the foam films were stabilized by proteins (BSA in our experiments, but we tried successfully other proteins as well) many droplets, or white blood cells, easily stuck to the water−air interface and remained entrapped within the film after its formation. One should note that experiments with *wetting films* (see the previous subsection) can be performed *without any surfactants.*

Other Methods. *Surface and Interfacial Tension Measurements.* The surface tension of the protein solutions was measured by the Wilhelmy plate method on a digital tensiometer K10T (KRÜSS, Germany). The interfacial tension was measured by a du Noüy ring method on the same equipment. The plate and the ring used in these measurements were made of platinum.

Zeta-Potential of Particles. The ζ-potential of latex particles was determined in Zetasizer IIC equipment (Malvern Instruments, U.K.) for measuring the electrophoretic mobility. A 0.01 M NaCl solution was used as a background electrolyte in these experiments. Since the particle size was much larger than the Debye screening length, $\kappa^{-1} \approx 3$ nm, the Smoluchowski equation was used for calculation of the ζ-potential from the measured electrophoretic mobility.[37]

Numerical Procedures for Data Interpretation

The numerical procedures in the cases of solid sphere and deformable droplet are different; hence they are described separately below.

Solid Sphere in Wetting Film. Figure 1a presents a digitized image of a spherical particle and the surrounding meniscus in wetting film, observed in reflected monochromatic light. Figure 4 shows a vertical cross section of the particle and the reconstituted meniscus profile of the same system. The magnitude of the three-phase contact angle, θ, can be found from the intersection of the *extrapolated* meniscus profile and the circumference representing the particle surface.

The shape of the meniscus can be restored from the interference pattern observed in reflected light (Figure 1a). A detailed physical analysis of the reflectivity of a thin dielectric film is presented in Chapter 1 of the classical book *Principles of Optics* by Born and Wolf.[38] According to this analysis, the intensity of the reflected light, measured by a detector (photomultiplier, CCD-camera, eye, etc.), depends on the difference in the optical paths of the two light beams, which are reflected from the two surfaces of the liquid film (the multiple reflection being negligible). Since the optical path difference is constant everywhere in the plane-parallel film far from the particle, these film regions seem homogeneous in brightness when observed in reflected light. On the other hand, interference fringes are observed in the regions where the layer changes its thickness (i.e., in the meniscus region close to the particle). The extrema in the intensity of the reflected light correspond to the condition[38]

$$Z_k = k\,\frac{\lambda_0}{4n_W} \qquad k = 0, 1, 2, ... \tag{1}$$

where Z_k is the local thickness of the water film. Here k is the order of interference and k is even for bright fringes and odd for dark fringes. n_W denotes the refractive index of the aqueous phase. From the recorded images one can determine the radial coordinate r_k corresponding to each fringe of order k. We developed an image analysis computer program, which calculated the average intensity of the reflected light over a circular fringe, centered at the axis of symmetry of the meniscus. In this way a precise determination of the radii of the interference minima and maxima is accomplished. Thus, the coordinates, Z_k and r_k, of several points from the meniscus surface are found.

The shape of the meniscus is theoretically described by the Laplace equation of capillarity, which for axisymmetrical systems can be written in the form (see, e.g., ref 39)

$$\frac{\mathrm{d}\sin\psi}{\mathrm{d}r} + \frac{\sin\psi}{r} = -\frac{\Delta P_{W/A}}{\sigma_{W/A}} + \frac{\Delta\rho_{W/A}g}{\sigma_{W/A}}Z \tag{2}$$

$$\frac{\mathrm{d}Z}{\mathrm{d}r} = \tan\psi = \frac{\sin\psi}{\sqrt{1-\sin^2\psi}} \tag{3}$$

Here Z denotes the local height of the meniscus profile, r is the radial coordinate, ψ is the running slope angle of the meniscus, $\Delta P_{W/A} = P_W - P_A$, is the capillary pressure drop between the aqueous and gaseous phases, and $\sigma_{W/A}$ is the surface tension of the aqueous phase (Figure 1b). The second term on the right-hand side of eq 2 accounts for the gravity: $\Delta\rho_{W/A}$ is the mass density difference of the aqueous and gaseous phases and g is the gravity acceleration.

Hartland and Hartley[40] demonstrated that for computational purposes it is often more convenient to use the length of the generatrix of the water−air interface, S, as a running parameter. This is particularly important in the case of a large particle where the position of the three

---

[36] Scheludko, A.; Exerowa, D. *Kolloidn Zh.* **1959**, *165*, 148.

[37] Hunter, R. J. *Zeta Potential in Colloid Science*; Academic Press: New York, 1981.

[38] Born, M.; Wolf, E. *Principles of Optics*, 6th ed.; Pergamon Press: Oxford, 1993.

[39] Kralchevsky, P. A.; Danov, K. D.; Denkov, N. D. In *Handbook of Surface and Colloid Chemistry*; Birdi, K. S., Ed.; CRC Press: London, 1996.

[40] Hartland, S.; Hartley, R. W. *Axisymmetric Fluid-Liquid Interfaces*; Elsevier: Amsterdam, 1976.

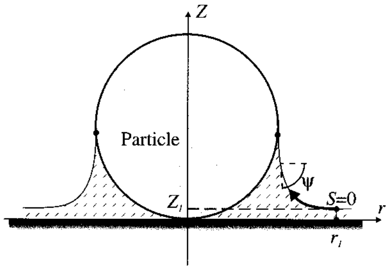

Figure 5. Schematic drawing illustrating the meaning of the geometrical variable, *S*, and its connection with the other variables.

phase contact line might be below the particle equator; see Figure 5. In this case the meniscus generatrix may have a turning point; i.e., there could be a certain range of radial coordinates, *r*, where the height of the profile, *Z*, acquires two values for the same *r*. By using the identities (see Figure 5)

$$\mathrm{d}r/\mathrm{d}S = \cos\psi \tag{4}$$

$$\mathrm{d}Z/\mathrm{d}S = \sin\psi \tag{5}$$

one can transform eq 2 to read

$$\frac{\mathrm{d}\psi}{\mathrm{d}S} = -\frac{\Delta P_{\mathrm{W/A}}}{\sigma_{\mathrm{W/A}}} + \frac{\Delta\rho_{\mathrm{W/A}}g}{\sigma_{\mathrm{W/A}}}Z - \frac{\sin\psi}{r} \tag{6}$$

The set of equations 4−6 for the three unknown functions $r(S)$, $Z(S)$, and $\psi(S)$ contains one unknown parameter, $\Delta P_{\mathrm{W/A}}$, and requires three boundary conditions to be solved. We choose (arbitrarily) $S = 0$ for the most outer dark interference fringe, corresponding to film thickness $Z_1 = (\lambda_0/4n_{\mathrm{W}}) = 102$ nm. Then the boundary conditions at this fringe can be written in the form

$$Z(S{=}0) = Z_1; \qquad r(S{=}0) = r_1; \qquad \psi(S{=}0) = \psi_1 \tag{7}$$

Note that in the boundary conditions (7) Z_1 is known while r_1 and ψ_1 are unknown values which must be determined (along with $\Delta P_{\mathrm{W/A}}$) from comparison of the calculated meniscus profile and the measured positions of the Newton fringes.

The fourth-order Runge−Kutta method[41] is used for solving eqs 4−6, and the merit function

$$\chi^2 = \sum_k [Z^{\mathrm{TH}}(r_k) - Z_k^{\mathrm{EXP}}(r_k)]^2 \tag{8}$$

is minimized for determination of r_1, ψ_1, and $\Delta P_{\mathrm{W/A}}$. Here $Z^{\mathrm{TH}}(r_k)$ is the theoretically calculated film thickness, while $Z_k^{\mathrm{EXP}}(r_k)$ values are found from the experimentally determined extrema of the interfered light (see eq 1). Summation is carried out over all observed fringes whose radii can be precisely measured. The three adjustable parameters are simultaneously varied using the Marquardt−Levenberg nonlinear least-squares method.[41] The experimental data and the best fit curve for one of the experiments with latex particles are shown in Figure 4.

Having found the three parameters ($\Delta P_{\mathrm{W/A}}$, r_1, and ψ_1), one can extrapolate the meniscus profile, obtained by solving the Laplace equation, toward small radial distances until its intersection with the particle surface. The three-phase contact angle is determined from the slope angles of the meniscus, ψ_{C}, and of the particle surface, φ_{C}, at the contact line $r = r_{\mathrm{C}}$ (see Figure 1b)

$$\theta = \varphi_{\mathrm{C}} - \psi_{\mathrm{C}} \tag{9}$$

The slope angle, φ_{C}, of the particle surface at the contact line is given by the geometrical relationship

$$\varphi_{\mathrm{C}} = \arcsin(r_{\mathrm{C}}/R) \tag{10}$$

where *R* is particle radius.

Experimental results with latex spheres, obtained by the procedure described above, are presented and discussed in the following section.

Droplet Trapped in Thin Foam Film. The analysis of the interference picture in the case of oil droplets (biological cells) is more complex compared to solid spheres, because one should take into account the deformation of the particles when trapped in the film; see Figure 2. It is necessary to use the Laplace equation of capillarity for both *air−water* and *oil−water* interfaces, in order to determine the shape of the deformed drop. From a computational viewpoint it is more convenient to entrap the droplets in *foam* films (Figure 2), because the system is symmetrical with respect to the plane of the film and the analysis is somewhat simpler. There are no essential difficulties to study deformable particles in wetting films (Figure 1), but for simplicity we will not consider this case.

It is deserving to note that, in principle, one could expect to see interference fringes in the central region (where the oil drop is located) of Figure 2a. The distance, *d*, between two consecutive fringes can be estimated to be $d \approx \lambda_0/(8n_{\mathrm{W}} \tan\psi)$, where ψ is the running slope angle. It turns out that the distance between two consecutive fringes becomes so small in a certain region close to the periphery of the drop (where the meniscus is steeper) that the fringes cannot be resolved in the microscope. On the other hand, the fringes located very close to the center of the image (where the meniscus slope is small again, see Figure 2b) cannot be well recognized, because their radii are around the resolution limit of the microscope (0.5 μm). For similar reasons one cannot distinguish interference fringes in the central region of Figure 1, where the latex particle is located.

For a foam film the Laplace equation of capillarity, which describes the shape of the two foam film surfaces, can be written in the form[39]

$$\frac{\mathrm{d}}{\mathrm{d}r}\left(\frac{Z_j'}{\sqrt{1 + Z_j'^2}}\right) + \frac{Z_j'}{r\sqrt{1 + Z_j'^2}} = -\frac{\Delta P_{\mathrm{W/A}}}{\sigma_{\mathrm{W/A}}} + (-1)^j \frac{\Delta\rho_{\mathrm{W/A}}g}{\sigma_{\mathrm{W/A}}} Z_j \tag{11}$$

$$Z_j' \equiv \mathrm{d}Z_j/\mathrm{d}r \tag{12}$$

Here the subscript *j* designates the lower ($j = 1$) and the upper ($j = 2$) meniscus. The remaining notations are the same as in eqs 2 and 3. Note that eqs 11 and 12 are counterparts to eqs 2 and 3, respectively.

The gravity term, $(-1)^j\Delta\rho_{\mathrm{W/A}}gZ_j/\sigma_{\mathrm{W/A}}$, in eq 11 implies some asymmetry of the foam film with respect to the plane $z = 0$. However, the numerical calculations showed that this term is 4 orders of magnitude smaller compared to the capillary pressure term, $\Delta P_{\mathrm{W/A}}/\sigma_{\mathrm{W/A}}$, for foam films. Therefore, the gravity term can be omitted in eq 11 without any loss of accuracy and the system can be considered as being symmetrical with respect to the midplane of the film.

---

(41) Press, W. H.; Teukolsky, S. A.; Vetterling, W. T.; Flannery, B. P. *Numerical Recipes in C. The Art of Scientific Computing*, 2nd ed.; Cambridge University Press: New York, 1992.

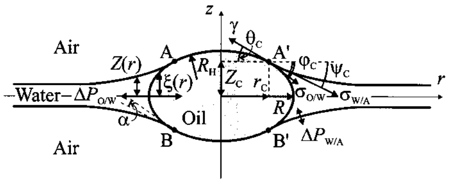

Figure 6. Schematic cross section of oil drop entrapped in symmetrical foam film. R denotes the equatorial radius of the deformed drop, r_C is the radius of the asymmetrical oil–water–air film, and R_H is the radius of curvature of the asymmetrical film. $Z(r)$ is the function describing the shape of the air–water interface and $\xi(r)$ describes the oil–water interface. $\Delta P_{O/W} = (P_O - P_W)$ and $\Delta P_{W/A} = (P_W - P_A)$ are the capillary pressures at the two interfaces.

The meniscus shape can be determined from eqs 11 and 12 and the measured radii of the interference fringes. The numerical procedure is practically the same as that described above for solid spheres. The merit function given by eq 8 is minimized to determine the adjustable parameters including the capillary pressure, $\Delta P_{W/A}$.

One should note that the foam film becomes planar far from the oil droplet due to the presence of a positive disjoining pressure, which presents a repulsive force (per unit area) between the two foam film surfaces.[32–35] The disjoining pressure in protein-stabilized films is determined mainly by the electrostatic and steric repulsive forces between the protein layers adsorbed on the two opposing film surfaces (there is also an additional contribution of the attractive van der Waals force, but it is smaller in magnitude for stable films). Although the disjoining pressure is important to ensure the stability of the foam film, it does not affect the used numerical procedure for analysis of the interference pattern. Indeed, the influence of the disjoining pressure on the shape of the film surfaces becomes negligible at a local film thickness larger than ca. 10 nm (the Debye screening length, κ^{-1}, is about 1 nm in the experiments with oil drops and about 3 nm in those with latex spheres). On the other hand, the interference fringes used for determination of the contact angle correspond to a local film thickness of 102 nm and larger (cf. eq 1). For this reason eq 11, which is applied for analysis of the interference pattern, does not include a disjoining pressure term.

Let us consider now the shape of the entrapped drop; see Figures 2 and 6. We use the so-called "membrane approach"[32–35,39] to describe the thin aqueous films formed between the oil drop and the gaseous phase in the regions of contact (these correspond to the arcs AA′ and BB′ in Figure 6). In other words, these asymmetrical oil–water–air films will be regarded as mathematical surfaces. At the contact line, $r = r_C$, the film that covers the drop (AA′ or BB′) meets the drop–water interface, $\xi(r)$, and the outer meniscus water–air, $Z(r)$, forming a contact angle, α (Figure 6).

The shape of the oil–water interface is also governed by the Laplace equation of capillarity, eqs 11 and 12. The only difference is that the function describing the generatrix of the oil–water interface, $\xi(r)$, must substitute $Z(r)$ and the respective quantities for the oil–water interface, $\Delta P_{O/W}$, $\sigma_{O/W}$ and $\Delta\rho_{O/W}$, should be used. For micrometer-sized droplets the gravity deformation of the oil–water interface is negligible; i.e., the second term in the right-hand side of eq 11 can be omitted without loss of accuracy. Due to the symmetry of the system with respect to the plane $Z = 0$, we can consider only the upper half of the drop and of the foam film ($Z > 0$). Also, the two caps on the drop (AA′ and BB′, respectively) can be considered as parts of spherical surfaces. After the above substitutions eqs 11 and 12 can be integrated by using the boundary condition

$$\xi' = -\infty \quad \text{at} \quad r = R \tag{13}$$

to obtain

$$\frac{d\xi}{dr} = \frac{b(1 - r^2/R^2) - 1}{\sqrt{1 - r^2/R^2}\sqrt{2b - 1 - b^2(1 - r^2/R^2)}} \tag{14}$$

where

$$b \equiv \frac{\Delta P_{O/W} R}{2\sigma_{O/W}} \tag{15}$$

It is convenient to introduce a new variable, Φ, through the relationship

$$m \sin^2 \Phi \equiv 1 - \frac{r^2}{R^2} \tag{16}$$

$$m \equiv \frac{2b - 1}{b^2} \tag{17}$$

After subsequent integration of eq 14 with the boundary condition $\xi(r{=}R) = 0$, one obtains the following expression for the shape of the oil–water interface

$$\xi(r) = R\int_0^{\Phi} \frac{1 - bm \sin \Phi}{b\sqrt{1 - m \sin^2 \Phi}}\, d\Phi = R[E(\Phi,m) - \sqrt{1 - m}F(\Phi,m)] \tag{18}$$

Here $F(\Phi,m)$ and $E(\Phi,m)$ are elliptic integrals of the first and second kind, respectively, defined through the expressions[42]

$$F(\Phi,m) \equiv \int_0^{\Phi} \frac{dx}{\sqrt{1 - m \sin^2 x}} \tag{19}$$

$$E(\Phi,m) \equiv \int_0^{\Phi} \sqrt{1 - m \sin^2 x}\, dx \tag{20}$$

$$0 < m < 1$$

Besides, the volume of the deformed drop can be found by integration of the profile $\xi(r)$

$$V = 2\pi\int_R^{r_C} r^2 \frac{d\xi}{dr}\, dr + 2V_{SC} \tag{21}$$

where V_{SC} is the volume of the spherical cap of the drop (above and below the planes AA′ and BB′ in Figure 6, respectively). Using eq 18 one obtains

$$V = \frac{2\pi R^3}{3}[(4 - 2m - 3\sqrt{1 - m})E(\Phi_C,m) - (1 - m)F(\Phi_C,m) + (m/2)\sin(2\Phi_C)\sqrt{1 - m \sin^2 \Phi_C}] + \frac{2\pi}{3}[2R_H^{\,2}(R_H - \sqrt{R_H^{\,2} - r_C^{\,2}}) - r_C^{\,2}\sqrt{R_H^{\,2} - r_C^{\,2}}] \tag{22}$$

where R_H denotes the radius of curvature of the drop caps (see Figure 6) and $\Phi_C = \Phi(r_C)$; see eq 16.

We are now prepared to formulate the set of equations which must be solved to completely describe the system. The geometrical requirement for intersection of the water–

---

(42) Abramowitz, M.; Stegun, I. A. *Handbook of Mathematical Functions*; Applied Mathematics Series, Vol. 55; National Bureau of Standards: Washington, DC, 1964; Chapter 17 (reprinted by Dover Publications: New York, 1968).

air interface with the drop–water interface at the contact line reads

$$(Z_C)_{W/A} = (\xi_C)_{DROP} \qquad (23)$$

where $(Z_C)_{W/A}$ is the height of the water–air interface at the contact line, obtained by extrapolation of experimentally measured meniscus profile, while $(\xi_C)_{DROP}$ is the height of the oil drop surface at the contact line. From eq 18 we have

$$(Z_C)_{W/A} = (\xi_C)_{DROP} \equiv R[E(\Phi_C,m) - \sqrt{1-m}\,F(\Phi_C,m)] \qquad (24)$$

Another relationship can be found by integrating the Laplace equation of capillarity which describes the shape of the drop–water interface ($r_C < r < R$) and can be written in the form

$$\sigma_{O/W}\frac{1}{r}\frac{d}{dr}(r\sin\varphi) = \Delta P_{O/W} \qquad (25)$$

The integration of eq 25 over r in the range from R to r_C leads to the expression

$$\sigma_{O/W}(r_C\sin\varphi_C - R) = \frac{1}{2}\,\Delta P_{O/W}(r_C^{\,2} - R^2) \qquad (26)$$

where φ_C is the slope angle of the oil–water interface at the contact line (see Figure 6). The capillary pressure at the oil–water interface, $\Delta P_{O/W}$, can be expressed through the capillary pressures at the water–air interface, $\Delta P_{W/A}$, and across the asymmetrical oil–water–air film, ΔP_F

$$\Delta P_{O/W} = \Delta P_F - \Delta P_{W/A} = \frac{2\gamma}{R_H} - \Delta P_{W/A} \qquad (27)$$

where γ is the film tension of the asymmetrical oil–water–air film (see Figure 6). From eqs 26 and 27 one can obtain the following expression

$$\sigma_{O/W}\left(\sin\varphi_C - \frac{R}{r_C}\right) = \frac{r_C^{\,2} - R^2}{2r_C}\left(\frac{2\gamma}{R_H} - \Delta P_{W/A}\right) \qquad (28)$$

which was used in the numerical calculations.

Two other relations stem from the interfacial tension vectorial balance at the three-phase contact line.[35,43] In principle, this balance should include a term accounting for the line tension. This effect can be taken into account in our consideration, but it was found with other systems to be rather small.[43] If the effect of the line tension here is also negligible, the horizontal and vertical projections of the balance of the interfacial tensions read (see Figure 6)[43]

$$\sigma_{W/A}\cos\psi_C + \sigma_{O/W}\cos\varphi_C = \gamma\cos\theta_C \qquad (29)$$

$$\sigma_{W/A}\sin\psi_C + \sigma_{O/W}\sin\varphi_C = \gamma\sin\theta_C \qquad (30)$$

where ψ_C and θ_C are respectively the slope angles of the water–air interface and of the droplet caps at the contact line.

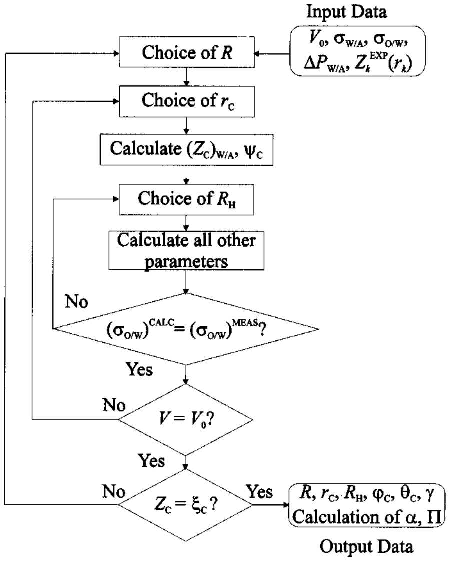

Figure 7. Basic block-scheme of the numerical procedure including three minimization loops. There is a limited range of values for V_0 in which the procedure is convergent.

From geometrical consideration one has an additional relationship between θ_C, r_C, and R_H

$$\sin\theta_C = r_C/R_H \qquad (31)$$

Finally, we utilize in the numerical procedure the fact that the drop volume, V, must be the same for a given droplet at different capillary pressures and different deformations (see below for details)

$$V(\Delta P_{W/A}) = V_0 = \text{const} \qquad (32)$$

where V is given by eq 21.

Hence we obtained a set of six equations, (23) and (28)–(32), for six unknown quantities (R, r_C, R_H, φ_C, θ_C, γ) at a given capillary pressure. The block-scheme of the used calculation procedure is shown in Figure 7. The input data for the procedure are V_0, $\sigma_{W/A}$, $\sigma_{O/W}$, $\Delta P_{W/A}$, and the shape of the water–air interface $Z_k(r_k)$, obtained from the interference fringes around the droplet. The numerical procedure includes three iterative optimization loops which correspond to the following requirements:

(i) The calculated interfacial tension of the oil–water interface must be equal to the value, which is measured independently by a tensiometer.

(ii) The volume of the droplet must be equal to a given value, V_0 (eq 32). The procedure used to find the value of V_0 is explained below.

(iii) The water–air interface must meet the oil–water interface at the contact line (eq 23).

The solution of the set of equations provides values of the unknown parameters and allows determination of the drop shape. In addition, one can calculate three other important quantities characterizing the system: (1) the disjoining pressure (force per unit area) that stabilizes the asymmetrical oil–water–air film covering the droplet caps

$$\Pi \equiv \frac{2\sigma_{W/A}}{R_H} - \Delta P_{W/A} = \frac{2\sigma_{W/A}}{r_C}\sin\theta_C - \Delta P_{W/A} \qquad (33)$$

Equation 33 can be derived, e.g., as a vertical balance of the pressures acting on the upper surface of the asym-

---

[43] Ivanov, I. B.; Kralchevsky, P. A.; Nikolov, A. D. *J. Colloid Interface Sci.* **1986**, *112*, 97. Ivanov, I. B.; Kralchevsky, P. A.; Dimitrov, A. S.; Nikolov, A. D. *Adv. Colloid Interface Sci.* **1992**, *39*, 77.

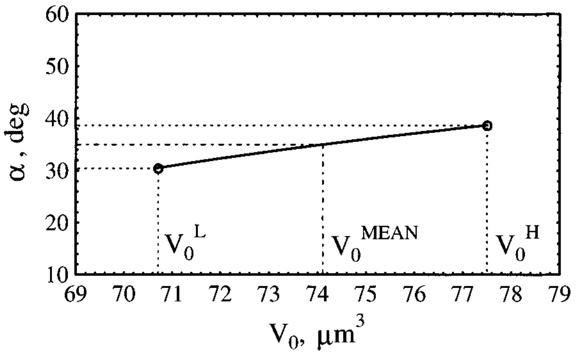

Figure 8. Calculated values of the contact angle, α, as a function of the presumed drop volume, V_0, fixed values for all other parameters. All points are calculated for the droplet shown in Figure 2a, at a capillary pressure $\Delta P_{W/A} = 158$ Pa. The range of values of V_0, for which the set of eqs 23 and 28−32 has a solution, is bounded by the values V_0^L and V_0^H; V_0^{MEAN} is equal to $(V_0^L + V_0^H)/2$. This range defines the error in the calculated contact angle: ±4° (the horizontal dashed lines).

metrical film; (2) the contact angle film-meniscus, α, which is given by a counterpart of eq 9

$$\alpha = \varphi_C - \psi_C \tag{9'}$$

(3) the work of adhesion[2] between the surface of the oil droplet and the water−air interface:

$$W = \sigma_{O/W} + \sigma_{W/A} - \gamma \tag{34}$$

Note, that W does not coincide with the interaction free energy of the film, Δf, which is another quantity used in the thermodynamics of thin liquid films.[32−34] The relationship between W and Δf is given by the expression

$$W \equiv -(\Delta f + \Pi h) \tag{35}$$

The second term in the right-hand side of eq 35 is usually negligible compared to the first one and, hence, $W \approx -\Delta f$.

In this way we can calculate all the geometrical and thermodynamic parameters characterizing the system.

The choice of the constant V_0 in eq 32 requires some additional explanations. In principle, one can measure directly the equatorial radius of the deformed drop, R, and use it as an input parameter in the computational procedure, instead of using eq 32. However, our calculations showed that the accuracy of the microscopic measurement of R is insufficient for this purpose—very small variation in the value of R (e.g., within ±100 nm, which is well below the resolution of the optical microscopy) leads to a large variation in the calculated values of the contact angle or to the absence of solution of the set of eqs 23 and 28−31.

To overcome this problem we used a more complex (but more accurate) numerical procedure. Let us assume that the error in determination of the drop volume, V_0^{EXP}, by optical microscopy is $\pm\Delta V_0^{EXP}$. We studied numerically how the solution of the set of eqs 23 and 28−32 would behave, depending on the value of ΔV_0^{EXP}. It turned out that the set of eqs 23 and 28−32 had a solution only in a relatively narrow range of values, $V_0^{MEAN} \pm \Delta V_0$, which is always confined within the framework of the experimentally determined volume, $V_0^{EXP} \pm \Delta V_0^{EXP}$. For the image shown in Figure 2a, the range of possible values for the drop volume (for a numerical solution to exist) is 74.1 ± 3.4 μm^3; see Figure 8. This variation (±3.4 μm^3) corresponds to an error in R of the order of ±60 nm. Within this range, there is a certain change of the calculated contact angle, α, and the maximum possible variation is $\Delta\alpha = \pm 4°$ (Figure 8). We checked this conclusion for a given drop at different capillary pressures, $\Delta P_{W/A}$, and found that the curve in Figure 8 did not depend appreciably on $\Delta P_{W/A}$. In all cases V_0^{MEAN} coincided with the optically determined value, $V_0^{EXP} \pm \Delta V_0^{EXP}$, in the framework of the experimental error.

Hence, we adopted the following procedure for more precise determination of the drop volume, V_0. On the basis of optical information we determined approximately the value of V_0^{EXP} and started varying it. At a given capillary pressure, $\Delta P_{W/A}$, the solution of the set of equations existed only in a range, bounded by two values, V_0^L and V_0^H (see Figure 8). To decrease the error, we took the arithmetic mean of V_0^L and V_0^H to obtain V_0^{MEAN} (for the given capillary pressure) and then averaged the latter value over all capillary pressures studied. Finally, calculations of the contact angle were performed with this averaged value. In other words we accepted that V_0 is equal to the averaged value of V_0^{MEAN}.

Results and Discussion

Micrometer-Sized Latex Particles. The results for the measured contact angles of six types of latex spheres are shown in Table 1. Each of the mean values shown in Table 1 is averaged over more than 15 measurements with at least 5 different particles of the same type. Two or three independent experiments were performed on each sample, and the results of these measurements coincided in the framework of the experimental error.

The experimental data for two of the samples (sulfate latex of mean diameter 2.07 μm and chloromethyl latex of mean diameter 1.55 μm) are presented in Figure 9. As seen from Table 1 and Figure 9, both the results for a given particle and the results for different particles are scattered within ± 2−5°. Therefore, we have not registered any detectable heterogeneity among the different particles in these samples. The scattering of the results for a given particle could be due (i) to the inevitable experimental inaccuracy in the measurement of the positions of the interference fringes or (ii) to some heterogeneity of the particle surface, which might lead to a hysteresis of the contact angle. One should note, that the particle size is an important parameter in the calculations, and an error in the used mean particle radius would result in a systematic error in the calculated contact angle.

Several interesting conclusions can be drawn from these results:

(i) Four of the samples (including the most typical sulfate latex) show contact angle in the range between 54 and 61°, although all of them have a different kind and concentration of ionizable surface groups. The other two samples demonstrated somewhat smaller contact angles: 32.4° and 40.7°, respectively. All these values characterize the polystyrene latex spheres as moderately hydrophobic, as far as their contact angles are between the values corresponding to typically hydrophilic ($\theta \sim 0$) and typically hydrophobic particles ($\theta \sim 90°$ and above).

(ii) The chloromethyl/sulfate latex is notably less hydrophobic ($\theta = 32.4 \pm 3.5°$) than the other latex samples. Therefore, it could be recommended to use chloromethyl/sulfate latex in the cases when the hydrophobic attraction must be avoided.

(iii) One could expect that more charged particles should have more hydrophilic surface. However, the results shown in Table 1 do not imply any direct correlation between the magnitude of the contact angle and the magnitude of the particle ζ-potential or surface charge density. For instance, the contact angles of samples no. 440 (56°) and no. 472 (55° at pH = 10.8) are very close

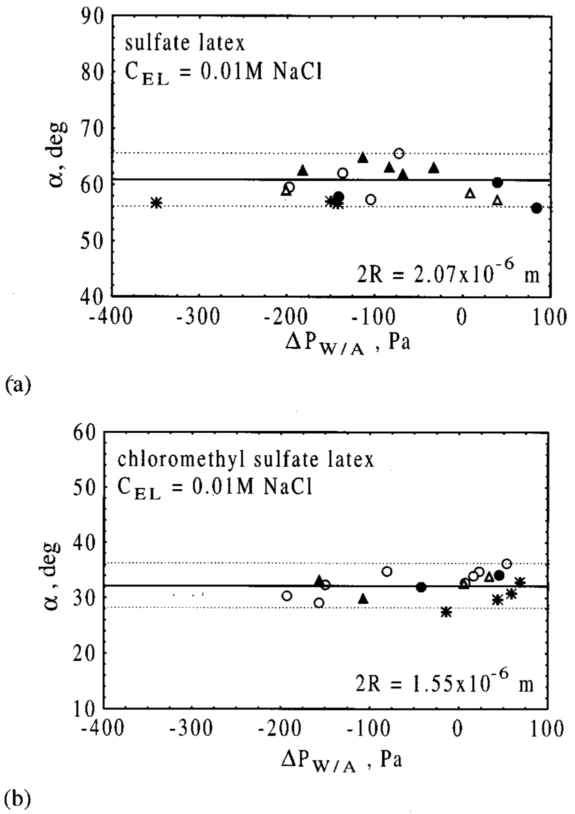

Figure 9. Measured contact angle of latex spheres: (a) sulfate latex, (b) chloromethyl sulfate latex. The different symbols correspond to results obtained on different particles. The horizontal dashed lines represent the standard deviation in the calculated contact angle. The capillary pressure, $\Delta P_{W/A}$, changes its sign from positive to negative with the shrinkage of the meniscus region around the particle, because the two principal radii of curvature of the water–air interface are of opposite sign (cf. Figure 1).

although the ζ-potential of the second type of particles is 2 times lower and their surface charge density is 1 order of magnitude higher. Therefore, the hydrophobicity of latex particles cannot be characterized on the basis of the electrical surface properties, such as ζ-potential and surface charge density.

It is worth mentioning that in principle the absorption of CO_2 from the atmosphere could change the pH of the studied samples during the experiment (especially of those having high pH values). We measured the pH of the suspensions before and after the ζ-potential measurements, and it was the same in the framework of the experimental accuracy (±0.1). It is difficult to assess at the present whether the absorption of CO_2 has influenced the results of the contact angle measurements.

Due to the simplicity and high accuracy of the present method it could be used as a standard procedure for characterization of latex particles.

Oil Droplet Entrapped in a Protein-Stabilized Liquid Film. A photograph of an oil droplet entrapped in a foam film is shown in Figure 2a. The protein-stabilized foam films were rather stable and relatively thick ($h \approx 80-90$ nm) probably due to dense protein layers adsorbed at the film surfaces. During the experiment we controlled the capillary pressure at the water–air interface, $\Delta P_{W/A}$, by sucking out small amounts of water from the Gibbs–Plateau border surrounding the foam film (which leads to increase of $\Delta P_{W/A}$) or by injection of water back into the Gibbs–Plateau border (decreasing of $\Delta P_{W/A}$). Several cycles of consecutive increasing and decreasing of capillary pressure were possible before the film rupture.

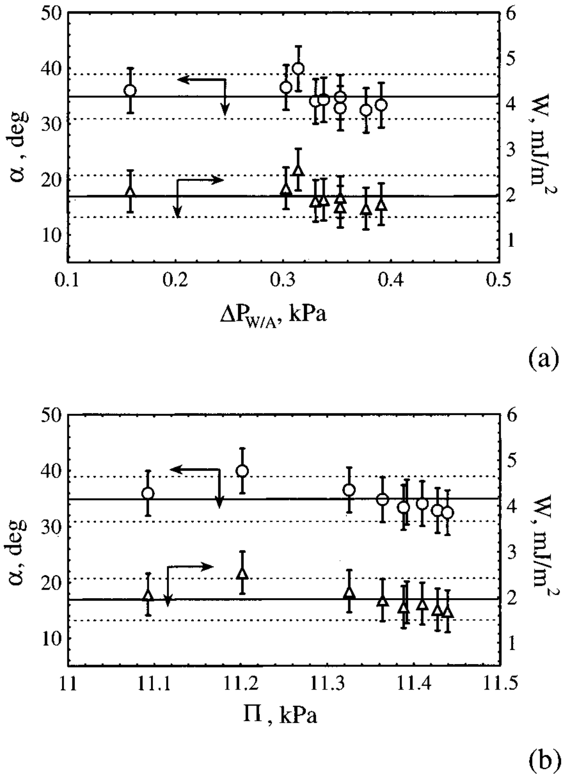

Figure 10. Contact angle, α, and energy of adhesion, W, as functions of the capillary pressure, $\Delta P_{W/A}$ (a), and of the disjoining pressure of the asymmetrical oil–water–air film, Π (b). The foam film is made from 2 wt % bovine serum albumin solution in 0.15 M NaCl at pH = 6.5. The oil drop is from purified soybean oil containing 0.1 wt % oleic acid as an additive; $V_0 = 74.1 \pm 3.4\ \mu m^3$ (calculated value).

The duration of one such cycle was typically between 5 and 10 min. The results from one cycle are presented in Figure 10a as a dependence of the contact angle film-meniscus, α, and of the adhesion energy, W, on the capillary pressure $\Delta P_{W/A}$. The volume of the droplet, $V_0 = 74.1 \pm 3.4\ \mu m^3$, was determined as explained in the previous section.

α and W in Figure 10b are presented as functions of the calculated disjoining pressure, Π, in the asymmetrical oil–water–air film. One sees from Figure 10 that the contact angle, α, is relatively large (around 35°) and does not depend on the capillary and disjoining pressures in the framework of the experimental accuracy. The adhesive energy, W, is equal to 1.7 mJ/m², and also does not depend notably on Π. The results from the other cycles of changing the capillary pressure on the same drop are very similar. The reproducibility of the values of α and W from measurements on different droplets of the same composition is within 10%.

One should note that the variation of the capillary pressure, $\Delta P_{W/A}$, is in a relatively wide range, typically between 150 and 400 Pa. However, the disjoining pressure, Π, varies in a relatively narrow range for a given droplet (cf. the horizontal axes in Figure 10). Indeed, the disjoining pressure depends mainly on the curvature of the thin asymmetrical film (see eq 33 where the second term in the right-hand side, $\Delta P_{W/A}$, turns out to be an order of magnitude smaller than the first one for our systems)

$$\Pi \propto 1/R_H \qquad (33')$$

The calculations show that in our experiments, R_H varies in a relatively narrow range of values for a given droplet and, hence, Π changes very slightly. On the other hand, the disjoining pressure is substantially different for droplets of different size—the smaller the droplets, the larger the disjoining pressure.

More extensive investigation of protein-stabilized oil droplets at different conditions is under way and will be published in the future. Such a study brings in information about the interactions between micrometer-sized drops, like those in batch emulsions.[44] As suggested by the experiments of Velev et al.,[45] the thinning pattern and the stability of micrometer-sized films could be substantially different in comparison with the films of larger diameter, which are studied in the conventional experimental cell.[36]

White Blood Cells Entrapped in Foam Film. In the following part of this section we illustrate the applicability of the film trapping technique (FTT) to another system, white blood cells (lymphocytes). Systematic study of biological cells by FTT will be presented later.[46] Our method might be useful to immunological studies where it was demonstrated[47] that the strong adhesion of the lymphocytes to the surface of the target cells is a necessary condition for the lymphocyte activation and immune response.

A photograph in reflected light of a human lymphocyte, trapped in a protein stabilized film, is shown in Figure 12a. In this case one sees two different sets of interference fringes: (i) an inner set, which is due to light reflected from the lower and upper spherical caps of the lymphocyte; (ii) an outer set, which is due to light reflected from the water−air interfaces around the lymphocyte. Set i is invisible in the case of oil droplets because the curvature of their caps is very high (the radius of curvature, R_H, is small), so the inner dark and bright fringes overlap with each other and could not be resolved by the microscope. The very low membrane tension of the lymphocytes results in a much stronger deformation of the cells; the radius of curvature of the two spherical caps is much larger now and the dark and bright fringes are well separated from each other and easily observable.

The procedure for shape analysis and contact angle determination of lymphocytes is not exactly the same as that described for oil droplets above. The main differences are as follows:

The radius of curvature of the spherical caps of an entrapped lymphocyte, R_H, can be determined directly from the inner set of interference fringes.

The condition for conservation of the particle volume is not used, because the lymphocyte can change its volume upon compression by release of a cytosol liquid into the surrounding solution.

The tension of the lymphocyte membrane is an adjustable parameter which is determined in the course of the calculations, because it cannot be measured independently. Furthermore, the membrane tension is not constant and can vary with changes in the capillary pressure.

Due to the biological activity of the living cells one could expect some of their properties (such as the adhesion energy, membrane tension, etc.) to be time-dependent.

The schematic cross section of the white blood cell is shown in Figure 12b. The adhesive energy is relatively high ($W = 1.6$ mJ/m^2), which might be due to the high affinity of the cell receptors to the IgG molecules adsorbed at the air−water interface. The calculated tension of the cell membrane is $\sigma_C = 1.8$ mN/m. This relatively high value (cf., e.g., the values quoted by Evans[48] for similar systems) can be explained by the large deformation of the cells entrapped in the film. The cell deformation leads to unruffling and stretching of the cell surface and corresponding increase of the membrane tension. The measured value of σ_C is of substantial interest, because the white blood cells are often subject to extreme deformations in the living organisms.[49] At the highest capillary pressures we sometimes observed disruption of the cytoplasmic membrane and lysis of the cells.

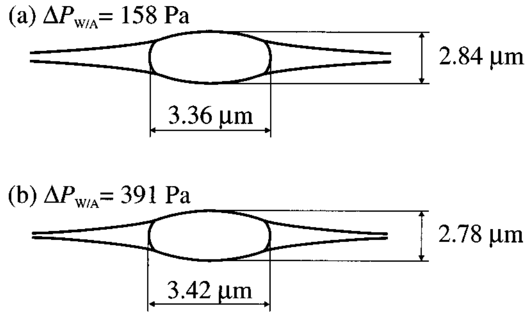

Figure 11. Reconstituted geometry of oil droplet entrapped in liquid film at two different values of the capillary pressure: (a) $\Delta P_{W/A} = 158$ Pa (b) $\Delta P_{W/A} = 391$ Pa.

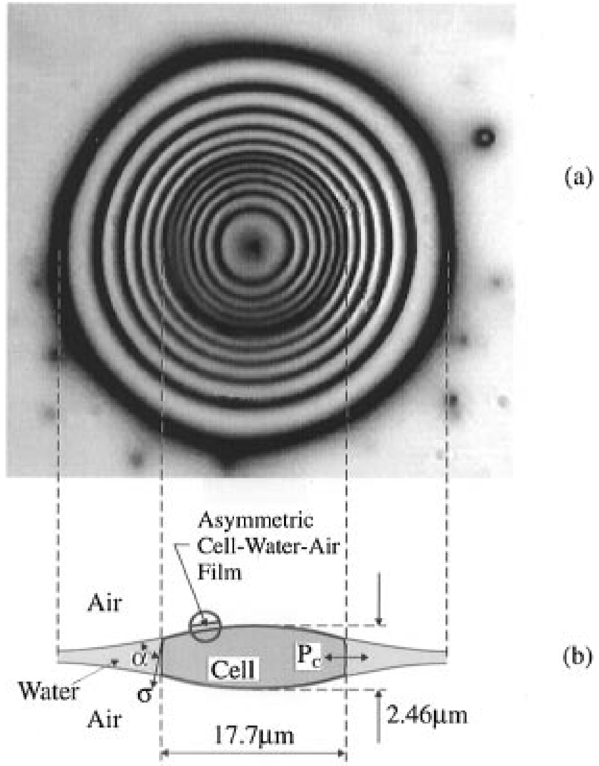

Figure 12. White blood cell trapped in thin liquid film: (a) digitized video image; (b) schematic cross section of the same cell. $\sigma = 1.8$ mN/m, $\alpha = 69.8°$, $\Pi = 1100$ Pa, $P_C = 1800$ Pa, $W = 1.6$ mJ/m^2.

Conclusions

The main conclusions of the present study can be summarized as follows:

A novel method for determination of particle contact angles is proposed (Figures 1 and 2). The method is called

---

[44] Denkov, N. D.; Petsev, D. N.; Danov, K. D. *Phys. Rev. Lett.* **1993**, *71*, 3226; *J. Colloid Interface Sci.* **1995**, *176*, 189.

[45] Velev, O. D.; Constantinides, G. N.; Avraam, D. G.; Payatakes, A. C.; Borwankar, R. P. *J. Colloid Interface Sci.* **1995**, *175*, 68.

[46] Ivanov, I. B.; et al. Manuscript in preparation.

[47] Mescher, M. F. *J. Immunol.* **1992**, *149*, 2402.

[48] Evans, E. In *Physical Basis of Cell-Cell Adhesion*; Bondgrand, P., Ed.; CRC Press: Boca Raton, FL, 1988; p 173.

[49] Darnell, J.; Lodish, H.; Baltimore, D. *Molecular Cell Biology*, 2nd ed.; Scientific American Books: New York, 1990; Figure 14-30.

"film trapping technique" (FTT), because the particles are entrapped in a liquid film of equilibrium thickness smaller than the particle diameter. The contact angles are determined from analysis of the interference pattern, which appears when the system is observed in reflected monochromatic light.

FTT is applicable to solid and fluid particles of micrometer size. When applied to solid spheres, the method provides values for the three-phase contact angle particle–water–air (Figure 4). When applied to fluid (deformable) particles, the method provides values for the thermodynamic quantities characterizing the thin asymmetrical film, which appears at the contact of the particle with the surface of the larger film (Figure 6): contact angle film-meniscus, adhesive energy, disjoining pressure, film tension, etc. (Figures 10 and 11). Numerical algorithms and computer programs for analysis of the interference pattern are developed (see the Experimental Section and Figure 7).

The method requires relatively uncomplicated equipment: simple home-made experimental cells and a microscope allowing observation in reflected monochromatic light. The accuracy of the method is within several degrees for both solid and fluid particles (see Table 1 and Figures 9 and 10).

The contact angles of six types of polystyrene latex spheres are measured to be within the range between 32° and 61°. This characterizes the studied latex particles as intermediate between typically hydrophilic and hydrophobic particles (Table 1).

Illustrative results with deformable oil droplets and white blood cells are presented (Figures 10–12).

FTT can be used as a standard procedure for quantitative characterization of the hydrophobicity of latex and silica spheres. In addition, the method seems rather versatile, in so far it can be extended to measuring dynamic contact angles (advancing and receding), as well as different types of angles like particle–oil–air and particle–water–oil. Lipid vesicles present another type of particle that can be studied by FTT. The bending elasticity energy and the stretching constant[2] of lipid bilayers are two parameters that could be obtained by applying similar experimental and numerical procedures on vesicles. Our experiments showed that the method can be successfully applied for investigation of the adhesive energy, the membrane tension, and other properties of biological cells.

Materials Available Upon Request. Computer programs (written in C for IBM compatible PC/AT) for analysis of the interference pattern in the Film Trapping Technique and calculating the contact angles of solid spheres and deformable droplets are available from the author.

Acknowledgment. The help in formulating the numerical procedure for oil drop analysis and the fruitful discussions with Professor Peter A. Kralchevsky and Dr. Theodor Gurkov are gratefully acknowledged.

LA9605551